

Geometrical Constraints On Leptonic Unitarity Triangles

Mathieu Guigue^{1,*} and Lorenzo Restrepo^{1,2,†}

¹*Laboratoire de Physique Nucléaire et des Hautes Énergies, Sorbonne Université, Paris, France*

²*IPSA-DRII, 63 boulevard de Brandebourg, 94200 Ivry-sur-Seine, France*

(Dated: January 27, 2026)

The precision of the neutrino oscillation parameters measurements has improved and will continue to improve as the next-generation experiments become online. Beyond the more precise measurements of the mixing angles and phases used to parametrize the lepton mixing matrix, tests of its unitarity are of great interest. This paper studies how the amplitudes of the oscillation patterns can be used and combined to construct leptonic unitarity triangles.

I. UNITARITY TRIANGLES IN THE LEPTON SECTOR

The oscillation of the neutrinos from one flavour to another has been a well-established quantum phenomenon for the last three decades, since its discovery by the SNO [1] and Super-Kamiokande [2] experiments. These oscillations are generally described within the Pontecorvo-Maki-Nakagawa-Sakata (PMNS) framework, [3, 4] which involves a 3×3 unitary mixing matrix, for the three known neutrino types.

As neutrino oscillation physics enters a precision era, it can be of interest to test our more fundamental hypotheses, such as the unitarity of the PMNS matrix. The presence of heavier neutrinos could be described by a larger dimension mixing matrix from which only a 3×3 subset is the PMNS matrix: typically, the see-saw models [5] that would explain the neutrinos mass origin in a natural way, predict the existence of several heavy neutrinos mixing with the standard light neutrinos [6]. In such case, one can imagine that the 3×3 matrix describing the standard neutrinos oscillation is not unitarity, and thus the equation

$$UU^\dagger = U^\dagger U = \mathbb{1}_3, \quad (1)$$

doesn't hold. There are various ways to test unitarity, in particular via the search of suppressed leptons decays e.g. $\mu \rightarrow e\gamma$. The resulting constraint consists in the direct constraint on the off-axis terms of $U^\dagger U$ [6]. Alternatively, one can constrain the mixing matrix element ratios on the complex plane: these are called “unitarity triangles”. Such search is done extensively in the quark sector, where the multiple probes that exist allow to tightly constraint the allowed region for the apexes of these triangles [7].

This paper presents how constraints on unitarity triangles in the lepton sector can be obtained from the individual neutrino oscillation measurements without assuming unitarity of the PMNS matrix. Section II presents the oscillation probability expression useful for this work. Section III A describes the general procedure for construct-

ing unitarity triangles. The connection between the neutrino oscillation amplitudes and the unitary triangle is described in Section III B, while the constructed triangles are displayed in Section IV. Finally, Section V discusses the difficulty of extracting the oscillation amplitudes and therefore the construction of unitarity triangles, while providing some insights about possible remedies.

II. NEUTRINO OSCILLATION AND OSCILLATION AMPLITUDES

A. Neutrino oscillation probability

Neutrino oscillation arises from a mismatch between the neutrino flavour eigenstates $|\nu_\alpha\rangle$ by which neutrinos interact, and mass eigenstates $|\nu_i\rangle$ by which they propagate. Flavour eigenstates can be decomposed as a linear combination of mass eigenstates:

$$|\nu_\alpha\rangle = \sum_{i=1}^N U_{\alpha i}^* |\nu_i\rangle, \quad (2)$$

with $N \geq 3$ being the number of neutrino mass eigenstates and U being the generic lepton mixing matrix.

The probability of a neutrino of flavour α to oscillate into the flavour β depends exclusively on the mixing matrix elements, on the neutrino energy E and on the propagation length L . In all generality neutrino oscillation probability in vacuum can be expressed as:

$$\begin{aligned} P_{\alpha\beta}^{\text{full}} = & \frac{1}{n_\alpha n_\beta} \left[\left| \sum_j U_{\alpha j}^* U_{\beta j} \right|^2 \right. \\ & - \sum_{j < k} 4 \mathcal{R}e[U_{\alpha j}^* U_{\beta j} U_{\alpha k} U_{\beta k}^*] \sin^2\left(\frac{\Delta m_{jk}^2 L}{4E}\right) \\ & \left. + \sum_{j < k} 2 \mathcal{I}m[U_{\alpha j}^* U_{\beta j} U_{\alpha k} U_{\beta k}^*] \sin\left(\frac{\Delta m_{jk}^2 L}{2E}\right) \right], \quad (3) \end{aligned}$$

with the normalisation factor $n_\alpha = |\langle \nu_\alpha | \nu_\alpha \rangle|$. If the sum covers indeed all the possible neutrino families (including sterile neutrinos), then the normalisation factor should be equal to one $n_\alpha = 1$. Nevertheless, some authors prefer to leave the normalisation free to be as conservative

* mathieu.guigue@lpnhe.in2p3.fr

† lorenzo.restrepo@lpnhe.in2p3.fr

as possible [8]. On the other hand, the antineutrino oscillation probability is expressed like Eq. (3) but applying the complex conjugation to every matrix element $U_{\alpha i}$.

B. Relevance of a generic three neutrino analysis framework

Starting from Eq. (3), there can be various ways to test the unitarity of the 3×3 PMNS matrix U . For example, one can incorporate one or more sterile neutrinos in the oscillation probability and use this model within the oscillation analysis frameworks [9]. Alternatively one can choose to perform the usual three neutrino oscillation analysis, but using non-unitary parametrisations of U [10]. In the most general scenario, the oscillation probability can be written as:

$$P_{\alpha\beta}^{\text{full}} = \frac{1}{1 + \epsilon^{(1)}} (P_{\alpha\beta}^{3\nu} + \epsilon_{\alpha\beta}^{(2)}), \quad (4)$$

where $\epsilon^{(1)}$ is linked to the normalisation of the states, $P_{\alpha\beta}^{3\nu}$ is the three neutrino oscillation probability, and $\epsilon^{(2)}$ encodes other potential contributions from sterile neutrinos. Another possibility consists on constraining the unitarity normalisation $\epsilon^{(1)}$ or closure $\epsilon^{(2)}$, based on an underlying hypothesis.

In this paper we present a different approach. Indeed, the physical data measured by oscillation experiments should come from $P_{\alpha\beta}^{\text{full}}$, but usually the oscillation analyses assume 3 flavours ($P_{\alpha\beta}^{\text{full}} = P_{\alpha\beta}^{3\nu}$) and unitarity. If we allow small deviations from unitarity, Eq. (4) can be expanded as

$$P_{\alpha\beta}^{\text{full}} \simeq (P_{\alpha\beta}^{3\nu} + \epsilon_{\alpha\beta}^{(2)})(1 - \epsilon^{(1)}) \simeq P_{\alpha\beta}^{3\nu} + \epsilon_{\alpha\beta} \neq P_{\alpha\beta}^{3\nu}, \quad (5)$$

with $\epsilon_{\alpha\beta} = \epsilon^{(1)} P_{\alpha\beta}^{3\nu} + \epsilon_{\alpha\beta}^{(2)}$. So if the oscillation analyses are performed with only 3 neutrino families, it will be always possible to measure deviations from unitarity provided that the chosen parametrisation for U is flexible enough to incorporate them. These deviations come from the relaxed conditions on the matrix elements of U , and from the additional corrections $\epsilon_{\alpha\beta}$, for which we remain completely agnostic in this work.

In essence, unitarity violation could manifest itself on the measurements when performing a three neutrino analysis with a non-unitary parametrisation of U . Therefore, from now on we will place ourselves in a three neutrino working framework and we will simply denote $P_{\alpha\beta}^{3\nu}$ as $P_{\alpha\beta}$.

C. Oscillation probability amplitudes

The three neutrino oscillation probabilities can be made explicit for muon neutrinos disappearance ($\nu_\mu \rightarrow$

ν_μ), electron neutrino disappearance ($\nu_e \rightarrow \nu_e$) and electron neutrino appearance ($\nu_\mu \rightarrow \nu_e$):

$$\begin{aligned} P_{\mu\mu} = & \left(\sum_k |U_{\mu k}|^2 \right)^2 - 4|U_{\mu 1}|^2|U_{\mu 2}|^2 \sin^2(X_{12}) \\ & - 4|U_{\mu 1}|^2|U_{\mu 3}|^2 \sin^2(X_{13}) \\ & - 4|U_{\mu 2}|^2|U_{\mu 3}|^2 \sin^2(X_{23}), \end{aligned} \quad (6)$$

$$\begin{aligned} P_{ee} = & \left(\sum_k |U_{ek}|^2 \right)^2 - 4|U_{e 1}|^2|U_{e 2}|^2 \sin^2(X_{12}) \\ & - 4|U_{e 1}|^2|U_{e 3}|^2 \sin^2(X_{13}) \\ & - 4|U_{e 2}|^2|U_{e 3}|^2 \sin^2(X_{23}), \end{aligned} \quad (7)$$

$$\begin{aligned} P_{\mu e} = & - 4\mathcal{R}e(U_{\mu 1}^* U_{e 1} U_{\mu 2} U_{e 2}^*) \sin^2(X_{12}) \\ & + 2\mathcal{I}m(U_{\mu 1}^* U_{e 1} U_{\mu 2} U_{e 2}^*) \sin(2X_{12}) \\ & - 4\mathcal{R}e(U_{\mu 1}^* U_{e 1} U_{\mu 3} U_{e 3}^*) \sin^2(X_{13}) \\ & + 2\mathcal{I}m(U_{\mu 1}^* U_{e 1} U_{\mu 3} U_{e 3}^*) \sin(2X_{13}) \\ & - 4\mathcal{R}e(U_{\mu 2}^* U_{e 2} U_{\mu 3} U_{e 3}^*) \sin^2(X_{23}) \\ & + 2\mathcal{I}m(U_{\mu 2}^* U_{e 2} U_{\mu 3} U_{e 3}^*) \sin(2X_{23}), \end{aligned} \quad (8)$$

with $X_{ij} = \frac{\Delta m_{ij}^2 L}{4E}$ and $\Delta m_{ij}^2 = m_i^2 - m_j^2$ being the squared mass difference between two mass eigenstates i and j . The first term of muon and electron neutrinos disappearance is a normalization factor that is equal to 1 in the case of unitary matrix as of Eq. (1).

Experimentally, if one is capable of measuring these oscillation probabilities as a function of X_{ij} , the amplitudes of the oscillations could be extracted. For example, in the case of the muon neutrino disappearance, one could extract independent constraints on $|U_{\mu 1}|^2|U_{\mu 2}|^2$, $|U_{\mu 1}|^2|U_{\mu 3}|^2$, and $|U_{\mu 2}|^2|U_{\mu 3}|^2$. For convenience, we will denote the disappearance amplitudes

$$A_{\alpha,ij} = |U_{\alpha i}|^2|U_{\alpha j}|^2 \quad (9)$$

with $\alpha \in \{\epsilon, \mu, \tau\}$.

In the case of the appearance probabilities, we will denote

$$\mathcal{R}_{\alpha\beta,ij} = \mathcal{R}e(U_{\alpha i}^* U_{\beta i} U_{\alpha j} U_{\beta j}^*) \quad (10)$$

$$\mathcal{I}_{\alpha\beta,ij} = \mathcal{I}m(U_{\alpha i}^* U_{\beta i} U_{\alpha j} U_{\beta j}^*). \quad (11)$$

In reality, as it was pointed out in Ref. [11], given the values of the squared masses splitting, it might be difficult to disentangle between the $\sin^2(X_{13})$ and $\sin^2(X_{23})$ terms, and therefore measure independently their respective amplitudes. In the interest of the discussion, we will assume one can distinguish between these while leaving this point to Section V.

III. RELATIONSHIP BETWEEN OSCILLATION PROBABILITY AMPLITUDES AND UNITARITY TRIANGLES

A. Unitarity triangles construction

By construction, a 3×3 complex matrix has 18 independent parameters. In particle physics and in the context of the lepton mixing, additional constraints on these parameters can be added, such as the removal of unphysical phases due to lepton field rephasing. For now, we consider that the non-unitary neutrino mixing matrix has indeed 18 independent parameters. Testing the unitarity (1) of a matrix consists then in testing the validity of the following equations:

$$\sum_{\alpha} |U_{\alpha i}|^2 = 1, \quad (12)$$

$$\sum_i |U_{\alpha i}|^2 = 1, \quad (13)$$

$$\sum_i U_{\alpha i} U_{\beta i}^* = 0 \quad (\alpha \neq \beta), \quad (14)$$

$$\sum_i U_{\alpha i} U_{\alpha j}^* = 0 \quad (i \neq j). \quad (15)$$

Equations (12) and (13) relate to the probability normalization [8], while Eq. (14) and (15) are used to produce the so-called *leptonic unitarity triangles* as these equations can be seen from a geometrical point of view in the complex plane. In the case of 3 neutrino flavours and 3 mass eigenstates, these conditions can produce up to 6 triangles. Let's consider the following condition as one possible case:

$$\frac{U_{e1} U_{\mu 1}^*}{U_{e3} U_{\mu 3}^*} + \frac{U_{e2} U_{\mu 2}^*}{U_{e3} U_{\mu 3}^*} + 1 = 0 \quad (16)$$

which corresponds to Eq. (14) for $\alpha = e$ and $\beta = \mu$. Usually, one defines the quantities [12] $\rho_{e\mu}^{(1)}$ and $\eta_{e\mu}^{(1)}$ as, respectively, the negative value of real and imaginary parts of the first ratio in Eq. (16):

$$\rho_{e\mu} + i\eta_{e\mu} = -\frac{U_{e1} U_{\mu 1}^*}{U_{e3} U_{\mu 3}^*}. \quad (17)$$

The coordinates of $\rho_{e\mu} + i\eta_{e\mu}$ in the complex plane corresponds to the apex of a triangle, the other two being $(0,0)$ and $(0,1)$, one of the sides of the triangle being normalized to a length of 1 by convention. Note that the apex of the triangle can also provide information about CP violation. Indeed, if the apex is not on the real axis, then there must be an imaginary component coming from at least one CP violating parameter of U . We can also define the quantities $\rho'_{e\mu}$ and $\eta'_{e\mu}$ as:

$$\rho'_{e\mu} + i\eta'_{e\mu} = \frac{U_{e2} U_{\mu 2}^*}{U_{e3} U_{\mu 3}^*} + 1. \quad (18)$$

Testing the unitarity for this triangle therefore consists in verifying that the apex defined by $\rho_{e\mu} + i\eta_{e\mu}$ superimposes with the one defined by $\rho'_{e\mu} + i\eta'_{e\mu}$. Any deviation from unitarity would graphically cause a non-superimposition of the two apexes. The former triangle is particularly interesting as it involves only the electron and muon neutrinos, to which long-baseline experiments are sensitive and could therefore constrain.

B. Geometrical constraints from oscillation probability amplitudes

Neutrino oscillation experiments measure the oscillation probability usually as a function of the neutrino energy or the propagation length; therefore they are sensitive to the oscillation amplitudes $A_{\alpha,ij}$ in the case of disappearance experiments or $\mathcal{R}_{\alpha\beta,ij}$ and $\mathcal{I}_{\alpha\beta,ij}$ in the case of appearance experiments. As these experiments are mostly dedicated to the measurement of the mixing angles within the PMNS framework, they don't report their measurements of the oscillation amplitudes. Unitarity tests using these measurements have been extensively studied in the literature, especially in the context of the future long-baseline neutrino experiments [8, 11]. However, the procedure used in these studies usually consists in recasting the constraints on the mixing angles and the CP violation phase into e.g. $\rho_{e\mu}$ and $\eta_{e\mu}$ in order to test the unitarity, while the mixing angles used in the underlying analyses assumed the unitarity.

A natural question is therefore how will these constraints on the oscillation amplitudes appear in a $(\rho_{e\mu}, \eta_{e\mu})$ plane, similarly to the CKM one [7]? For example, what combination of constraints is required to produce e.g. a circle on this plane? Let's compute the radius R of a circle centred on $(\rho_{e\mu}, \eta_{e\mu}) = (0,0)$ and see how it can be expressed as a function of the oscillation amplitudes constraints. The radius R is defined as

$$R^2 = \rho_{e\mu}^2 + \eta_{e\mu}^2 = \frac{|U_{\mu 1}|^2 |U_{e1}|^2}{|U_{\mu 3}|^2 |U_{e3}|^2}, \quad (19)$$

which can be written as

$$R^2 = \rho_{e\mu}^2 + \eta_{e\mu}^2 = \frac{|U_{\mu 1}|^2 |U_{\mu 2}|^2 |U_{e1}|^2 |U_{e2}|^2}{|U_{\mu 2}|^2 |U_{\mu 3}|^2 |U_{e2}|^2 |U_{e3}|^2} = \frac{A_{\mu,12} A_{e,12}}{A_{\mu,23} A_{e,23}} \quad (20)$$

This expression shows that the constraints on several disappearance amplitudes can be combined into a circle in the $(\rho_{e\mu}, \eta_{e\mu})$ plane. Similarly, one can combine the constraints $A_{\mu,12}$, $A_{e,12}$, $A_{\mu,13}$ and $A_{e,13}$ into a circle centered on $(\rho'_{e\mu}, \eta'_{e\mu}) = (1,0)$ with a radius R' :

$$\begin{aligned} R'^2 &= (\rho'_{e\mu} - 1)^2 + \eta'^2_{e\mu} \\ &= \frac{|U_{\mu 1}|^2 |U_{\mu 2}|^2 |U_{e1}|^2 |U_{e2}|^2}{|U_{\mu 1}|^2 |U_{\mu 3}|^2 |U_{e1}|^2 |U_{e3}|^2} = \frac{A_{\mu,12} A_{e,12}}{A_{\mu,13} A_{e,13}}. \end{aligned} \quad (21)$$

From these expressions of R and R' , in order to constrain each circle one needs to measure 4 disappearance amplitudes. Moreover, it shows that the uncertainties on the

circle radius are directly related to the precision on each amplitude measurement; in other words, the precision on the radius is driven by the least precise amplitude measurement.

Constraints on the angles of the triangle or similarly on the slope of its sides are also possible as they arise from a constraint of $\eta_{e\mu}/\rho_{e\mu}$ or $\eta'_{e\mu}/(\rho'_{e\mu} - 1)$. Indeed, these ratios can be expressed as a function of the disappearance amplitudes:

$$\begin{aligned} \frac{\eta_{e\mu}}{\rho_{e\mu}} &= \frac{\mathcal{I}m\left(-\frac{U_{e1}U_{\mu1}^*}{U_{e3}U_{\mu3}^*}\right)}{\mathcal{R}e\left(-\frac{U_{e1}U_{\mu1}^*}{U_{e3}U_{\mu3}^*}\right)} = \frac{\mathcal{I}m\left(\frac{U_{e1}U_{\mu1}^*U_{e3}^*U_{\mu3}}{U_{e3}U_{\mu3}^*U_{e3}^*U_{\mu3}}\right)}{\mathcal{R}e\left(\frac{U_{e1}U_{\mu1}^*U_{e3}^*U_{\mu3}}{U_{e3}U_{\mu3}^*U_{e3}^*U_{\mu3}}\right)} \\ &= \frac{\mathcal{I}m\left(U_{\mu1}^*U_{e1}U_{\mu3}U_{e3}^*\right)}{\mathcal{R}e\left(U_{\mu1}^*U_{e1}U_{\mu3}U_{e3}^*\right)} = \frac{\mathcal{I}_{\mu e,13}}{\mathcal{R}_{\mu e,13}}, \end{aligned} \quad (22)$$

since $U_{e3}U_{\mu3}^*U_{e3}^*U_{\mu3} = |U_{e3}|^2|U_{\mu3}|^2$ is a real number. One can recognize the ratio between the amplitude of the $\sin(2X_{13})$ term and the amplitude of the $\sin^2(X_{13})$ term (up to a factor 2 and a minus sign since the amplitudes have opposite signs), which means that one can constrain the linear relationship between $\eta_{e\mu}$ and $\rho_{e\mu}$ using the measurement of the $\nu_\mu \rightarrow \nu_e$ and $\bar{\nu}_\mu \rightarrow \bar{\nu}_e$ X_{13} patterns. Similarly, the ratio $\eta'_{e\mu}/(\rho'_{e\mu} - 1)$ can be expressed as:

$$\begin{aligned} \frac{\eta'_{e\mu}}{\rho'_{e\mu} - 1} &= \frac{\mathcal{I}m\left(\frac{U_{e2}U_{\mu2}^*}{U_{e3}U_{\mu3}^*}\right)}{\mathcal{R}e\left(\frac{U_{e2}U_{\mu2}^*}{U_{e3}U_{\mu3}^*}\right)} \\ &= \frac{\mathcal{I}m\left(U_{\mu2}^*U_{e2}U_{\mu3}U_{e3}^*\right)}{\mathcal{R}e\left(U_{\mu2}^*U_{e2}U_{\mu3}U_{e3}^*\right)} = \frac{\mathcal{I}_{\mu e,23}}{\mathcal{R}_{\mu e,23}}, \end{aligned} \quad (23)$$

which can be constrained using only the measurements of $\mathcal{R}_{\mu e,23}$ and $\mathcal{I}_{\mu e,23}$.

C. Application: standard and generic unitary PMNS matrix

In the previous section we explained how the PMNS matrix elements can be combined to make geometrical unitarity constraints in the complex plane, in particular in the shape of circles and lines. But as we illustrated in Section II B, deviations from unitarity could only show up in the measurements if the parametrisation of U is non-unitary. Here we will compare the usual parametrisation adopted by the experiments with a more versatile one from Ref. [8].

If we assume that U is a $n \times n$ unitary matrix, it can be parametrised by $\frac{n \times (n-1)}{2}$ ($= 3$ for $n = 3$) mixing angles, and $\frac{n \times (n+1)}{2}$ ($= 6$ for $n = 3$) phases. Three of these phases can be removed due to lepton field rephasing, and two of them (the Majorana phases) do not play any role in the oscillation. Thus, a unitary parametrisation of the PMNS matrix involves three mixing angles θ_{ij} and one physical phase δ . The usual parametrisation adopted in

the oscillation analyses is the following:

$$U = \begin{pmatrix} 1 & 0 & 0 \\ 0 & c_{23} & s_{23} \\ 0 & -s_{23} & c_{23} \end{pmatrix} \begin{pmatrix} c_{13} & 0 & s_{13}e^{-i\delta} \\ 0 & 1 & 0 \\ -s_{13}e^{i\delta} & 0 & c_{13} \end{pmatrix} \begin{pmatrix} c_{12} & s_{12} & 0 \\ -s_{12} & c_{12} & 0 \\ 0 & 0 & 1 \end{pmatrix} \quad (24)$$

where $c_{ij} = \cos(\theta_{ij})$ and $s_{ij} = \sin(\theta_{ij})$. This parametrisation is unadapted to perform unitarity tests, because it will always verify the unitarity conditions defined by Eq. (12), (13), (14), and (15) by construction.

A possible approach consists in considering the general lepton mixing matrix without unitarity. Indeed, if we don't impose any constraint on U , there are in total 18 independent parameters (coming from the 9 complex matrix elements). Identically to the unitary case, five phases can be removed, which leaves us with 13 independent parameters for a general non-unitary parametrisation of U . We adopt the parametrization provided in Ref. [8]:

$$U \equiv \begin{pmatrix} |U_{e1}| |U_{e2}| e^{i\phi_{e2}} & |U_{e3}| e^{i\phi_{e3}} \\ |U_{\mu1}| |U_{\mu2}| & |U_{\mu3}| \\ |U_{\tau1}| |U_{\tau2}| e^{i\phi_{\tau2}} & |U_{\tau3}| e^{i\phi_{\tau3}} \end{pmatrix}, \quad (25)$$

with the values of the 4 phases ϕ_{e2} , ϕ_{e3} , $\phi_{\tau2}$ and $\phi_{\tau3}$ extracted from that paper to estimate the values of the relevant oscillation amplitudes.

Let us highlight the link between the phases from the parametrisations and the position of the apex of the unitarity triangle in the complex plane. The slope of the sides of the triangles are defined by Eq. (22) and (23). Translating this ratio in terms of the parametrisation in Eq. (25) gives:

$$\begin{aligned} \frac{\eta_{e\mu}}{\rho_{e\mu}} &= \frac{\mathcal{I}m\left(|U_{e1}||U_{\mu1}||U_{e3}|e^{-i\phi_{e3}}|U_{\mu3}|\right)}{\mathcal{R}e\left(|U_{e1}||U_{\mu1}||U_{e3}|e^{-i\phi_{e3}}|U_{\mu3}|\right)} \\ &= \frac{\sin(-\phi_{e3})}{\cos(-\phi_{e3})} = -\tan(\phi_{e3}), \end{aligned} \quad (26)$$

$$\begin{aligned} \frac{\eta'_{e\mu}}{\rho'_{e\mu} - 1} &= \frac{\mathcal{I}m\left(|U_{e2}|e^{i\phi_{e2}}||U_{\mu2}||U_{e3}|e^{-i\phi_{e3}}|U_{\mu3}|\right)}{\mathcal{R}e\left(|U_{e2}|e^{i\phi_{e2}}||U_{\mu2}||U_{e3}|e^{-i\phi_{e3}}|U_{\mu3}|\right)} \\ &= \frac{\sin(\phi_{e2} - \phi_{e3})}{\cos(\phi_{e2} - \phi_{e3})} = \tan(\phi_{e2} - \phi_{e3}), \end{aligned} \quad (27)$$

where the matrix element norms completely vanish from the equation. The same computation in terms of the usual unitary parametrisation from Eq. (24) gives:

$$\frac{\eta_{e\mu}}{\rho_{e\mu}} = \frac{\sin(\delta)}{\cos(\delta) + \frac{s_{12}s_{13}s_{23}}{c_{12}c_{23}}}, \quad (28)$$

$$\frac{\eta'_{e\mu}}{\rho'_{e\mu} - 1} = \frac{\sin(\delta)}{\cos(\delta) - \frac{c_{12}s_{13}s_{23}}{s_{12}c_{23}}}, \quad (29)$$

which is in agreement with Ref. [11]. These equations shows that in both cases the constraint on the slope of the apex is mainly driven by the CP violating phases of the parametrisation. In other words, the amount of CP violation is governed by the slope, which is the ratio between the imaginary and real parts of the apex coordinates.

IV. IMPLEMENTATION OF THE CONSTRAINTS ON A UNITARITY TRIANGLE

Unfortunately the constraints of the oscillation amplitudes are not usually provided by the collaborations. Therefore, we will assume experimental constraints on these quantities based on the global fits values [8, 11]. Indeed, the authors conveniently provide numerical values for their 3σ constraints on the squared matrix elements $|U_{\alpha i}|^2$; we will take the best fit values for computing the true values of the oscillation amplitudes. Tables I gives the numerical values of the assumed truth for the oscillation amplitudes of interest.

In addition, we assume a fixed 5 % error on each amplitude measurement. The decision to use arbitrary uncertainties instead of current ones arises from the desire to better observe their effects, particularly the intersection points between all the constraints. Let us point out that this precision is not completely unrealistic given the cumulated statistics in long-baseline neutrinos experiments like T2K: the total size of the muon neutrino samples of 455 events [13] would give a pure statistical precision of about 5 %. Clearly, the observations presented here should be further studied with more accurate estimations of the current and future precision on the parameters, but in this work they are meant to provide some insights.

A. Implementation framework

To confirm these observations, we use the Bayesian inference software called Stan [14] to build an a posteriori distribution on the $\rho_{e\mu}$ and $\eta_{e\mu}$ variables. Stan uses Hamiltonian Markov-chain Monte-Carlo techniques to efficiently explore high-dimension parameter spaces, which is useful in the case of complex geometrical shapes.

Contrary to previous work e.g. [8, 11] where the constraints on the mixing angles were used to construct these variables, we assume here that the real and imaginary parts of PMNS matrix complex elements are free (meaning a flat prior) and only constrained by the oscillation amplitudes measurements. The oscillation amplitudes e.g. $\mathcal{R}_{\mu e, 23}$ are then derived from these low-level matrix elements.

The a posteriori distribution on the PMNS matrix elements therefore consists in a set of flat priors on these matrix elements and a global likelihood which is the product of normal distributions with the difference between the derived oscillation amplitudes and the experimental constraints as mean value and the relative error of 5 %. Thanks to the Stan framework, the constraints on the matrix elements can then be recasted into constraints on $\rho_{e\mu} + i\eta_{e\mu}$ and $\rho'_{e\mu} + i\eta'_{e\mu}$ as complex numbers.

B. Disappearance amplitudes constraints

Figure 1 shows the constraints with only ν_μ and ν_e disappearance measurements e.g. $A_{\alpha, 12}$, $A_{\alpha, 13}$ and $A_{\alpha, 23}$ with $\alpha \in \{e, \mu\}$. As expected from Eq. (20) and (21),

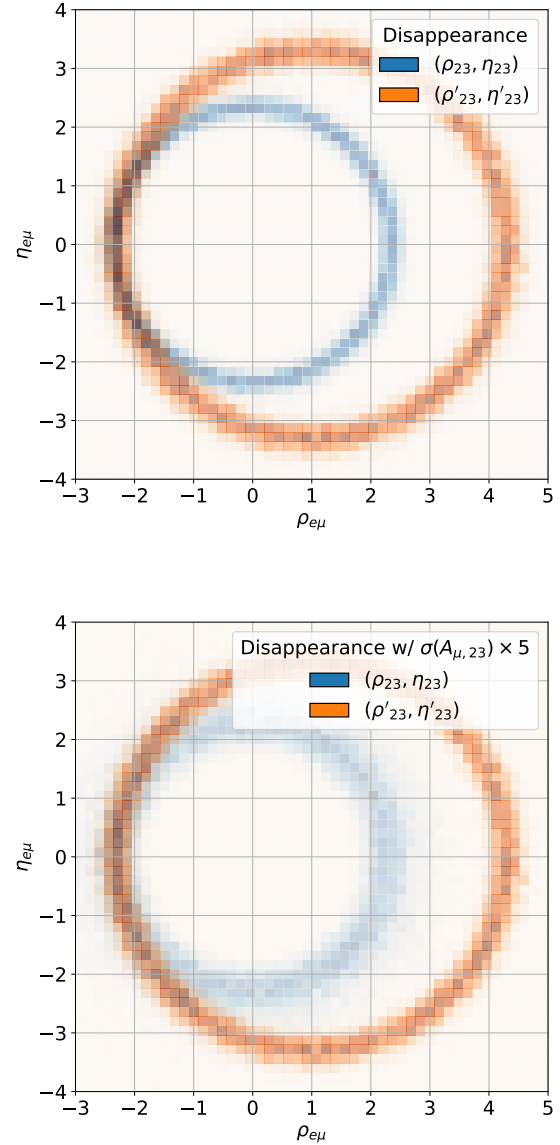


FIG. 1. Constraints on $(\rho_{e\mu}, \eta_{e\mu})$ Eq.(17) (blue) and $(\rho'_{e\mu}, \eta'_{e\mu})$ Eq. (18) (orange) when considering only constraints on the disappearance amplitude measurements. Top: the amplitude values are computed using Table I and the error on each amplitude is set to 5 %. Bottom: Same, but where the error on $A_{\mu, 23}$ is artificially increased by a factor of 5.

the constraint on each doublet $(\rho_{e\mu}, \eta_{e\mu})$ and $(\rho'_{e\mu}, \eta'_{e\mu})$ has a circular shape that only relates to the measurements of the 4 disappearance amplitudes. The bottom plot of Fig. 1 also shows the effect of the error on $A_{\mu, 23}$:

Disappearance constraints					
$A_{e,12}$	$A_{e,13}$	$A_{e,23}$	$A_{\mu,12}$	$A_{\mu,13}$	$A_{\mu,23}$
0.203476	0.014872	0.006622	0.0368095	0.045864	0.203868

Appearance constraints			
$\mathcal{R}_{\mu e,13}$	$\mathcal{I}_{\mu e,13}$	$\mathcal{R}_{\mu e,23}$	$\mathcal{I}_{\mu e,23}$
0.023270	0.0118569	-0.034740	-0.0119622

TABLE I. Mean values of the amplitudes assumed for the constraints in the unitarity plane. Top: values used for the disappearance constraints (Fig. 1). Bottom: values used for the appearance constraints (Fig. 2).

the radius uncertainty increases for the $(\rho_{e\mu}, \eta_{e\mu})$ circular shape, while leaving $(\rho'_{e\mu}, \eta'_{e\mu})$ unchanged as we expected from Eq. (20) and (21). The measurement and combination of the 6 amplitudes for the ν_μ and ν_e disappearance provide some information about the CP violation, as the intersection points between the blue and orange circles have a close to zero y-coordinate (although with an undetermined sign). Additionally, contrary to Ref. [8, 11], the direct usage of the oscillation amplitudes instead of the mixing angles doesn't present the typical double-circle induced by the θ_{23} octant degeneracy.

C. Appearance amplitudes constraints

Similarly, we can look at the impact of the appearance amplitudes constraints to the $(\rho_{e\mu}, \eta_{e\mu})$ plane.

Table I gives the mean values of these oscillation amplitudes. Assuming a typical error on these parameters of 5 %, it is possible to compute the expected range of the oscillation amplitudes and use them as constraints on the $(\rho_{e\mu}, \eta_{e\mu})$ coefficients. Figure 2 (top) shows the expected constraints from the appearance amplitude measurements: as expected, each set of measurements $\mathcal{R}_{\mu e,13}$ and $\mathcal{I}_{\mu e,13}$ (resp. $\mathcal{R}_{\mu e,23}$ and $\mathcal{I}_{\mu e,23}$) provides radial-shaped constraints on $(\rho_{e\mu}, \eta_{e\mu})$ (resp. $(\rho'_{e\mu}, \eta'_{e\mu})$). Since no constraint on the product of the matrix elements themselves is implied by these measurements, the line stretches from $(0, 0)$ (or $(1, 0)$) to infinity.

The additional constraints on e.g. the disappearance normalization values $(\sum_k |U_{ek}|^2)^2$ and $(\sum_k |U_{\mu k}|^2)^2$ allow to reduce the range of possible values of $\rho_{e\mu}$ and $\eta_{e\mu}$, as depicted in Fig. 2 (bottom). This second set of constraints is more similar to the ones presented in [8] as disappearance channel constraints, which indicates that the methodology employed there (a.k.a. the use of mixing angle constraints instead of oscillation amplitudes) implicitly includes normalization constraints from the appearance channels.

D. Combined constraints

Figure 3 shows unitarity constraint when putting together the appearance and disappearance measurements.

All the constraints combine into a point-like shape for both $(\rho_{e\mu}, \eta_{e\mu})$ and $(\rho'_{e\mu}, \eta'_{e\mu})$ with perfect overlap; with worse constraints on the measurements, one expects a wider shape. Figure 3 also shows the effect of a 50 % bias on the disappearance amplitude $\mathcal{R}_{\mu e,13}$: in this case, the apexes do not overlap meaning a break of unitarity.

V. DISCUSSION

A. Practical limitations

Let us finish this discussion with the observation that searching for a non-unitarity of the mixing matrix is way more complex in the context of neutrinos than for quarks. Indeed, the quark sector possesses multiple probes of the CKM matrix elements and its various phases. For instance, it is possible to measure precisely the decay of mesons, corresponding to measuring the transition from one quark to another and so the absolute value of a single CKM matrix element. Whereas the mostly accessible probe in the neutrino sector is their oscillation which involves between 2 and 4 PMNS matrix elements.

In practice, the experimental constraints on the oscillation amplitudes cannot be as clean as we assumed here; for example, the degeneracy between the $2 - 3$ and $1 - 3$ patterns in Eq. (6), (7) and (8) induced by the close values of Δm_{23}^2 and Δm_{13}^2 means that one can experimentally measure primarily $(|U_{\mu 1}|^2 + |U_{\mu 2}|^2) |U_{\mu 3}|^2$ from the oscillation pattern defined by Eq. (6). More realistic cases should be studied further to better understand the constraints one can have on the leptonic unitarity.

The studies performed in this work were made regarding the (e, μ) unitarity triangle. The primary reason is because the third row of the mixing matrix is hard to measure directly, as it involves τ neutrinos. Thus, for the moment, the primary focus should be to precisely measure independently the combination of the matrix elements of the first two rows of the mixing matrix.

B. Experimental strategy

This paper shows that certain combinations of oscillation amplitudes can give rise to geometrical constraints

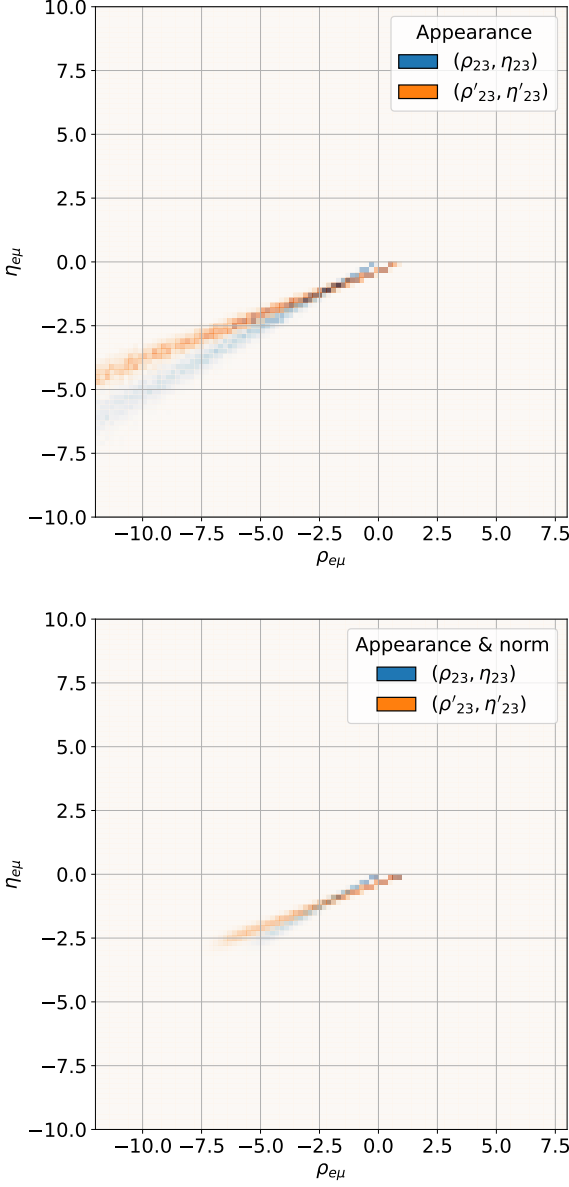


FIG. 2. Future constraints on $(\rho_{e\mu}, \eta_{e\mu})$ Eq. (17) (blue) and $(\rho'_{e\mu}, \eta'_{e\mu})$ Eq. (18) (orange) when considering constraints on the appearance amplitude measurements. Top: the amplitudes values are computed using Table I and the error on each amplitude is set to 5 %. Bottom: Same, but additional constraints on the $(\sum_k |U_{ek}|^2)^2$ and $(\sum_k |U_{\mu k}|^2)^2$ values are included as normal of mean value 1 and 5 % error.

on the unitarity triangle apex. In particular, the same oscillation amplitudes combinations that intervene in the disappearance probability amplitudes, control the circle-like constraints, and in particular the radius from Eqs. (20) and (21). Similarly, the oscillation amplitudes that intervene in the appearance probability, can be used to constrain the slope of the radial-shaped constraints. Up until now we assumed that these combinations could be measured by the oscillation experiments individually.

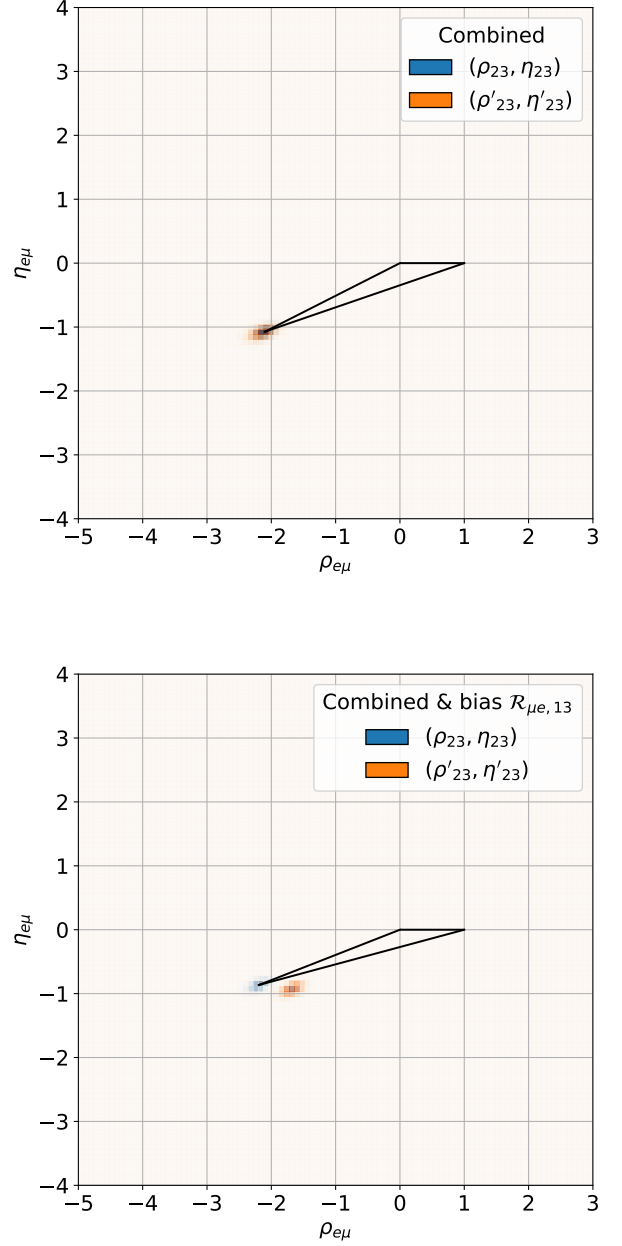


FIG. 3. Future constraints on $(\rho_{e\mu}, \eta_{e\mu})$ Eq. (17) (blue) and $(\rho'_{e\mu}, \eta'_{e\mu})$ Eq. (18) (orange) when considering all constraints on the appearance and disappearance amplitudes measurements. Top: the amplitudes values are computed using Table I and the error on each amplitude is set to 5 %. Bottom: Same, but a bias of 50 % is applied to $\mathcal{R}_{\mu e, 13}$.

But in a more practical scenario, is this experimentally feasible?

Neutrino oscillation experiments [15] have shown the following hierarchy between the mass splitting: $|\Delta m_{12}^2| \ll |\Delta m_{13}^2| \simeq |\Delta m_{23}^2|$, with a difference of almost two orders of magnitude. Depending on the value

of L/E , different terms can dominate in the oscillation probabilities. As an example, let us consider the electron neutrino disappearance probability from Eq. (7). In the regime where $X_{12} \sim \frac{\pi}{2}$, the X_{13} and X_{23} oscillations are very rapid with L/E , so they are averaged out in the probability. Therefore, the dominant term is proportional to $|U_{e1}|^2|U_{e2}|^2$. This is the regime where some electron disappearance experiments operate, like KamLAND and JUNO. But on the other hand, there is currently no muon neutrino disappearance experiment that operates in that regime, and that could therefore constrain $|U_{\mu 1}|^2|U_{\mu 2}|^2$ directly. This is due to the practical difficulty to do such an experiment. For example, for a muon neutrino beam with mean energy of 130 MeV, the far detector should be located at around 2100 km from the production site to detect the first oscillation maximum, which is more or less the distance between Tokyo and Beijing.

In the regime where $X_{13} \sim X_{23} \sim \frac{\pi}{2}$, the X_{12} term is too small to give rise to oscillations, so the dominant term is proportional to $|U_{e3}|^2(|U_{e1}|^2 + |U_{e2}|^2)$. Some electron disappearance experiments such as Daya Bay operate in this regime. It could be possible to disentangle between these two contributions if the second order terms are also constrained. Indeed, these terms are proportional to $|U_{e3}|^2|U_{ei}|^2$ with $i = 1$ or 2 depending on the mass ordering. In the muon neutrino sector, long baseline experiments such as T2K and NO ν A operate in that same regime. Consequently their muon disappearance measurements are sensitive to $|U_{\mu 3}|^2(|U_{\mu 1}|^2 + |U_{\mu 2}|^2)$ at first order. In the coming years, long baseline experiments such as T2HK and DUNE will be able to tightly constrain this quantity, and maybe even have access to the second order terms, which are proportional to $|U_{\mu 3}|^2|U_{\mu i}|^2$.

Long baseline experiments also measure electron neutrino and antineutrino appearance. The electron neutrino appearance is described by the probability in Eq. (8). In the regime $X_{13} \sim X_{23} \sim \frac{\pi}{2}$ the probability is driven by at least 3 terms: one proportional to $\sin^2(X_{i3})$ (with $i = 1$ or 2), another proportional to $\sin(2X_{i3})$ and the last one proportional to $\sin(2X_{12})$. The oscillation amplitudes are also entangled in this case, like for the muon disappearance measurements. Consequently, in order to constrain them, other inputs are necessary, like the electron and muon disappearance amplitudes.

In summary, if experiments such as Daya Bay are able to measure second-order combinations like $|U_{e3}|^2|U_{ei}|^2$, then all of the electron disappearance amplitudes $A_{e,ij}$ could be constrained. If not, then the matrix element

amplitudes $|U_{ei}|$ have to be constrained individually. For this, solar neutrino experiments can be proven useful, such as SNO and Borexino, as they are sensitive to the quantity $|U_{e2}|^2(|U_{e1}|^2 + |U_{e2}|^2) + |U_{e3}|^4$ at first order. For the muon row, things are more complicated because the measurements come almost exclusively from long baseline experiments. Therefore, there is no experiment capable of constraining $|U_{\mu 1}|^2|U_{\mu 2}|^2$, and there are no inputs equivalent to the solar neutrinos for the electron row. To constrain the last muon disappearance amplitude $A_{\mu,12}$ and the appearance amplitudes used in equations (22) and (23), more complete feasibility studies should be performed by long baseline analysers. Most probably the electron row measurements need to be used as inputs for this.

VI. CONCLUSIONS

As pointed out in the current literature, using the mixing angle constraints as input for unitarity triangle drawings can provide insights about the sensitivity of experiments, but cannot be a unitarity test. Adopting a pedagogical approach more than a pure quantitative one, this paper explores an ideal scenario where the oscillation amplitudes are independently measured with a precision of 5 %. Here we have demonstrated how the oscillation amplitudes measurements involving muon and electron neutrinos should be combined to draw unitarity triangles and constrain unitarity. Each geometrical figure in the $(\rho_{e\mu}, \eta_{e\mu})$ plane is derived as a product or ratio of pure disappearance or pure appearance oscillation probabilities components.

To construct unitarity triangles for neutrinos, the oscillation experiments are encouraged to measure and report the amplitudes of multiple oscillations terms, in order to disentangle the contributions from each term. Additionally, if instead one had access to the measurement of a different combination of matrix elements or better to the measurement of individual elements, it would help draw different constraints on the triangles themselves.

ACKNOWLEDGMENTS

The authors would like to thank Boris Popov and Marco Martini for the helpful comments and the kind guidance. This research was funded by IN2P3/CNRS and the French “Agence nationale pour la recherche” under grant number ANR-21-CE31-0008.

[1] Q. R. Ahmad, R. C. Allen, et al. *Direct Evidence for Neutrino Flavor Transformation from Neutral-Current Interactions in the Sudbury Neutrino Observatory*, Phys. Rev. Lett. **89** (1), 011301 (2002).

[2] Y. Fukuda, T. Hayakawa, et al. (Super-Kamiokande), *Evidence for oscillation of atmospheric neutrinos*, Phys. Rev. Lett. **81**, 1562 (1998).

- [3] Z. Maki, M. Nakagawa, and S. Sakata, *Remarks on the Unified Model of Elementary Particles*, Progress of Theoretical Physics **28** (5), 870 (1962).
- [4] V. Gribov and B. Pontecorvo, *Neutrino astronomy and lepton charge*, Phys. Lett. B **28** (7), 493 (1969).
- [5] H. Fritzsch, M. Gell-Mann, and P. Minkowski, *Vectorlike weak currents and new elementary fermions*, Phys. Lett. B **59** (3), 256 (1975).
- [6] S. Antusch, C. Biggio, et al., *Unitarity of the leptonic mixing matrix*, J. High Energ. Phys. **2006** (10), 084–084, arXiv:hep-ph/0607020 [hep-ph] (2006).
- [7] J. Charles, A. Höcker, et al., *CP violation and the CKM matrix: assessing the impact of the asymmetric B factories*, EPJ C **41** (1), 1 (2005).
- [8] S. A. R. Ellis, K. J. Kelly, and S. W. Li, *Current and future neutrino oscillation constraints on leptonic unitarity*, J. High Energ. Phys. **2020** (12), 068, arXiv:2008.01088 [hep-ph] (2020).
- [9] P. Coloma, J. López-Pavón, et al., *New physics from oscillations at the dune near detector, and the role of systematic uncertainties*, J. High Energ. Phys. **2021** (8), 65 (2021).
- [10] A. M. G. Trzeciak, H. Nunokawa, and A. A. Quiroga, *Impact of unitarity violation on sensitivity of the leptonic cp phase at hyper-kamiokande and dune*, J. High Energ. Phys. **2025** (11), 059 (2025).
- [11] S. A. R. Ellis, K. J. Kelly, and S. W. Li, *Leptonic Unitarity Triangles*, Phys. Rev. D **102** (11), 115027, arXiv:2004.13719 [hep-ph] (2020).
- [12] For convenience, we usually drop the ⁽¹⁾.
- [13] K. A. et al. (T2K collaboration), *Results from the T2K experiment on neutrino mixing including a new far detector μ -like sample*, Phys. Rev. Lett. **135**, 261801, arXiv:2506.05889 [hep-ex] (2025).
- [14] B. Carpenter, A. Gelman, et al., *Stan: A Probabilistic Programming Language*, Journal of Statistical Software, Articles **76** (1), 1 (2017).
- [15] I. Esteban, M. C. Gonzalez-Garcia, et al., *NuFit-6.0: updated global analysis of three-flavor neutrino oscillations*, J. High Energ. Phys. **2024** (12), 216, arXiv:2410.05380 [hep-ph] (2024).